Chemical Engineering Journal 149 (2009) 102–109

Contents lists available at ScienceDirect

Chemical Engineering Journal

journal homepage: www.elsevier.com/locate/cej

Modeling catalytic oxidation of lean mixtures of methane–air in a packed-bed reactor

S.A. Shahamiri, I. Wierzba*

Department of Mechanical and Manufacturing Engineering, University of Calgary, 2500 University Drive, NW, Calgary, AB, Canada T2N 1N4

ARTICLE INFO

Article history:
Received 27 February 2008
Received in revised form
20 September 2008
Accepted 22 September 2008

Keywords:
Methane
Lean mixtures
Catalytic oxidation
Packed-bed reactor

ABSTRACT

A mathematical model developed for simulation of combustion of preheated lean homogeneous methane–air mixtures in an adiabatic catalytic packed bed is described. The unsteady one-dimensional model includes inter-phase heat and mass transfers, longitudinal mass dispersion in the gas phase and longitudinal conduction and radiation heat transfer modes. The solid and gas phases are assumed not to be in local thermal equilibrium. Multi-step reaction mechanisms are employed for both the surface and gas phase chemical reactions. The surface reaction mechanism for the oxidation of methane on Pt includes 36 elementary surface reactions and 11 surface adsorbed species. The gas phase reaction mechanism includes 28 elementary reactions and 21 species. The governing equations are the unsteady equations of conservation of mass, chemical species and separate energy equations for solid and gas phases. These equations were solved using the commercial CFD code 'Fluent' and a number of modifying subroutines especially are developed to include the equations of surface reactions in the computations.

The model has been used to investigate the effects of operational conditions such as the mixture inlet temperature (600–1250 K), approach velocity (0.5–15 m/s) and equivalence ratio (0.15–0.5) on the oxidation of methane within both the catalytic and non-catalytic packed-bed reactors under adiabatic conditions. The calculated values of methane conversion showed good agreement with the corresponding available experimental data. Moreover the amount of heat release at different inlet velocities was calculated and the optimum value discussed.

1. Introduction

The potential and significance of catalytic combustion is well known. Catalytic combustion offers distinct advantages over conventional combustion. It has been well recognized that the rates of oxidation reactions within very lean mixtures of common gaseous fuels in air can be increased significantly through the presence of some catalytic materials [1]. Complete combustion in catalytic devices can be achieved at lower temperatures resulting in very low NOx and other emissions [2]. It would be possible then to utilize the energy release from gaseous fuel mixtures that are normally considered to be un-exploitable waste (e.g. very lean fuel–air mixtures, some biogases, etc.) [3,4]. The use of catalytic combustors has two primary objectives: to carry out stable combustion for low concentrations of fuel in air and to attain levels of pollutant emissions substantially below those possible with conventional ones.

The principles of catalytic combustion and the general developments in the field have been described in a number of review articles [2,5,6]. The technology and database needed to incorporate catalytic reactions in practical heat and power systems are expanding rapidly. There are attempts to apply catalytic combustors in gas turbines, furnace and boilers [2,7]. So far, most of the applications of catalyst in practical combustion systems, whether to enhance the rate of combustion processes or to complete the desirable oxidation of pollutants in the exhaust gas have involved expensive and relatively rare metals such as platinum and palladium. Over the years, many of experimental and theoretical investigations were conducted to improve the understanding of catalytic systems. Major types of catalytic reactors that can be used for combustion are of the monolith and packed-bed types that operate on essentially the similar principles. Most of the research reported in the open literature appears to have involved monolith type reactors.

Several methods have been proposed for simulating the combustion process in this type of catalytic reactors [6–10]. However, due to the complexity of the physical and chemical phenomena involved and their interactions, many of the existing theoretical models were developed for special applications and narrow range of operating conditions. Many of these models also neglect some

* Corresponding author. Tel.: +1 403 220 4156; fax: +1 403 282 8406.
E-mail addresses: sa.shahamiri@ucalgary.ca (S.A. Shahamiri), iwierzba@ucalgary.ca (I. Wierzba).

1385-8947/$ – see front matter © 2008 Elsevier B.V. All rights reserved.
doi:10.1016/j.cej.2008.09.046

Nomenclature

a_v	specific geometric surface
a_c	catalytic surface area to volume ratio
A	pre-exponential factor (mol, cm, s)
c	constant pressure specific heat
d_p	pellet diameter
$D_{i,m}$	diffusivity of species i
E	activation energy
h	convective heat transfer coefficient
H_i	enthalpy of species i
J_H, J_D	heat and mass transfer factors
k	thermal conductivity
k_f	forward Arrhenius rate
$k_{i,m}$	convective mass transfer coefficient of species i
L	reactor length
M_i	molar mass of species i
p	pressure (Pa)
q_{rad}	radiative heat flux
$\dot{R}_g$	species production rate in gas phase
$\dot{R}_s$	species production rate on surface
S_0	initial sticking coefficient
T	temperature
u	axial velocity
X_i	molar concentration of species i
Y_i	mass fraction of species i

Greek symbols

β	temperature exponent
ε	porosity
Φ	equivalence ratio
Γ	surface site density
μ	viscosity
Θ	surface coverage fraction
ρ	density
υ	stoichiometric coefficient

Subscript

g	gas phase
s	surface, solid

important aspects of the processes involved, such as for example to neglect the gas phase reactions [11] or to assume that the gas and solid phases are in thermal equilibrium [12]. Also, the majority of models treated the surface and gas reactions as global reactions of the Arrhenius type [6]. More recently reported models [8–10] include 2D and some 3D treatment of the flow within the monolith and introduce multi-step mechanisms for catalytic surface reactions.

A packed-bed type reactor was considered. Such a reactor tends also to be easier to make and cheaper to employ than the monolith type. Moreover, such a reactor was employed in our previous experimental investigation of the effectiveness of made-in-house metal oxide catalysts and experimental data are available to validate the model developed. Moreover, it can be considered as a better alternative for experimental research of many complex transport and chemical processes taking place within catalytic combustors [12,13]. However, in comparison with monolith type reactors there is much less information available on catalytic combustion in such a reactor in general, and there is only a few mechanisms proposed for catalytic oxidation of lean mixtures of methane and air on Pt.

The objective of the present contribution is to develop a model of reactive flow within a catalytic packed bed which would include adequate heat and mass transfer models and consider more realistic multi-step mechanisms for both simultaneous gas phase and surface reactions. Such a model can be applied to investigate the effects of key operational parameters on fuel oxidation processes within the packed-bed reactor, including the effect of fuel composition (e.g. the presence of diluents). It can also be used in combination with experimental data in deriving much needed kinetic data for catalytic surface reactions when employing different catalysts.

2. Physical and mathematical description of the problem

A schematic diagram of the packed bed being considered is shown in Fig. 1. A premixed, preheated homogeneous fuel/air mixture enters a cylindrical reactor packed with catalytic or non-catalytic pellets. The bed is initially at a uniform temperature. The fuel and oxygen diffuse from the bulk fluid to the catalyst surface where they are adsorbed and react. The products formed leave the surface via a desorption process and travel from the surface to the gas mixture via mass diffusion. A portion of the heat released due to surface reactions increases the solid temperature, while the remainder is transferred to the gas phase. The heat received by the gas phase may be high enough to promote the gas phase reactions. The three modes of heat transfer (conduction, convection and radiation) contribute jointly to the transport of heat within the reactor. Conduction redirects heat from the downstream to the upstream regions of the bed that contributes to an additional preheating of the fuel–air mixture. Convective heat transfer provides heat exchange between the solid and gas phases while the radiation mode becomes important mainly at sufficiently high levels of temperature.

The transport processes taking place within the reactor are complex and the following assumptions are employed in the developed model. The reactor operates adiabatically and at atmospheric pressure. The flow in the reactor is assumed to be one-dimensional. The gas and solid are not in local thermal equilibrium. Therefore, separate energy equations are considered for each phase. Radiation heat transfer in the gas phase is considered to be negligible in comparison to the solid pellets radiation. The thermophysical properties of the gas species are functions of the local temperature and composition while those of the pellets are assumed to be uniform and temperature independent. Based on these assumptions the governing conservation equations of mass, energy, and species are as follows:

$$\frac{\partial \rho_g}{\partial t} + \frac{\partial(\rho_g u_g)}{\partial x} = 0 \tag{1}$$

$$\rho_g \frac{\partial Y_{g,i}}{\partial t} + \rho_g u_g \frac{\partial Y_{g,i}}{\partial x} = -\rho_g D_{i,m} \frac{\partial^2 Y_{g,i}}{\partial x^2} + \frac{k_{i,m}}{\varepsilon} a_c \rho_g (Y_{s,i} - Y_{g,i}) + M_i \dot{R}_{g,i} \quad (i = 1, \ldots, N_g) \tag{2}$$

$$k_{i,m} \rho_g (Y_{g,i} - Y_{s,i}) = M_i \dot{R}_{s,i} \quad (i = 1, \ldots, N_g) \tag{3}$$

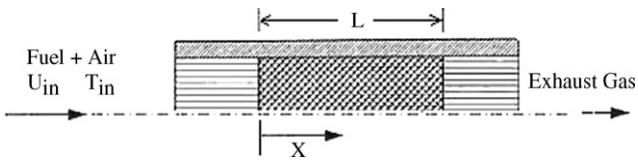

Fig. 1. Schematic diagram of reactor.

$$\rho_g c_g \frac{\partial T_g}{\partial t} + \rho_g c_g u_g \frac{\partial T_g}{\partial x} = -k_g \frac{\partial^2 T_g}{\partial x^2} + \frac{h}{\varepsilon} a_v (T_s - T_g) + \sum_{j=1}^{N_g} M_j \dot{R}_{g,j} H_j \tag{4}$$

$$\rho_s c_s \frac{\partial T_s}{\partial t} = -k_s \frac{\partial^2 T_s}{\partial x^2} + \frac{\partial q_{rad}}{\partial x} + \frac{h}{1-\varepsilon} a_v (T_g - T_s) + \sum_{j=1}^{N_s} \frac{a_c}{1-\varepsilon} M_j \dot{R}_{s,j} H_j \tag{5}$$

Ideal gas law:

$$\rho_g = \frac{RT_g}{pM_g} \tag{6}$$

The diffusion coefficients, $D_{i,m}$ for each species (Eq. (2)) are obtained using the kinetic theory of gases and dilute mixtures assumption that is valid for lean mixtures. The value of the thermal conductivity, k_s, (Eq. (5)) is obtained from Ref. [14]. The diffusion approximation for radiation is used to consider the effect of radiation heat transfer with q_{rad} (in Eq. (5)) calculated from:

$$q_{rad} = -\frac{16\sigma T^3}{3\beta} \frac{\partial T}{\partial x} \tag{7}$$

where σ is the Stefan–Boltzmann constant, 5.67×10^{-8} W/(m^2 K), and β is the extinction coefficient calculated from Ref. [15]:

$$\beta = 1.5\varepsilon_r (1-\varepsilon) \frac{S_r}{d_p} \tag{8}$$

where ε_r is the emissivity of the pellets, ε is the porosity of the bed and S_r is the scaling factor calculated as

$$S_r = 1 + 1.84(1-\varepsilon) + 3.15(1-\varepsilon)^2 + 7.2(1-\varepsilon)^3, \quad \varepsilon > 0.3 \tag{9}$$

The convective heat transfer coefficient, h, (Eqs. (4) and (5)) and convective mass transfer coefficient, $k_{i,m}$, (Eqs. (2) and (3)) are calculated using the corresponding Colburn factors, J_H and J_D [16] as

$$h = J_H \rho u c_g \left(\frac{\mu c_g}{k_g} \right)^{2/3} \tag{10}$$

$$k_{i,m} = J_D u \left(\frac{\mu}{\rho D_{i,m}} \right)^{2/3} \tag{11}$$

where

$$J_H = J_D = \begin{cases} 0.91 Re^{-0.51} \varphi, & 0.01 < Re < 50 \\ 0.61 Re^{-0.41} \varphi, & 50 < Re < 1000 \end{cases} \tag{12}$$

Re is defined as

$$Re = \frac{\rho u_g}{a_v \varphi \mu} \tag{13}$$

where φ is the pellets shape factor (e.g. it equals 0.91 for cylindrical pellets [16]).

The boundary and initial conditions are:

- *Boundary conditions*:

$$\text{At } x = 0: \quad T_g(x,t) = T_{g,inlet}, \quad h(T_g(x,t) - T_s(x,t)) = -k_s \frac{\partial T_s(x,t)}{\partial x}, \quad Y_g(x,t) = Y_{g,inlet} \tag{14}$$

$$\text{At } x = L: \quad \frac{\partial T_g(x,t)}{\partial x} = 0, \quad \frac{\partial T_s(x,t)}{\partial x} = 0, \quad \frac{\partial Y_{g,i}(x,t)}{\partial x} = 0 \tag{15}$$

- *Initial condition*:

$$\text{At } t = 0: \quad T_g(x) = T_{g,inlet}, \quad T_s(x) = T_{g,inlet}, \quad Y_i(x) = Y_{i,inlet} \tag{16}$$

2.1. Reaction rate for gas phase and surface reactions

If the reaction mechanism for the gas phase includes N_g species and K_g elementary reactions the rate of depletion or creation of species i in the gas phase, $\dot{R}_{g,i}$ (Eqs. (2) and (4)) is calculated as

$$\dot{R}_{g,i} = \sum_{k=1}^{K_g} \nu_{ik} k_{fk} \prod_{j=1}^{N_g} [X_j]^{\nu'_{jk}} \quad (i = 1, \ldots, N_g) \tag{17}$$

where ν_{ik} and ν'_{jk} are the stoichiometric coefficients, X_j is the molar concentration of species j and k_{fk} is the Arrhenius rate of kth reaction

$$k_{fk} = A_k T^{\beta_k} \exp\left(-\frac{E}{RT} \right) \tag{18}$$

In order to determine the evolution of X_j a set of ordinary differential equations (ODEs) is solved at each flow time step

$$\frac{d[X_j]}{dt} = \dot{R}_{g,j} \quad (j = 1, \ldots, N_g) \tag{19}$$

Similarly, the rate of depletion or generation of species $\dot{R}_{s,i}$ on the surface, i (Eqs. (3) and (5)), is calculated as

$$\dot{R}_{s,i} = \sum_{k=1}^{K_s} \nu_{ik} k_{fk} \prod_{j=1}^{N_g+N_s} [X_j]^{\nu'_{jk}} \quad (i = 1, \ldots, N_g + N_s) \tag{20}$$

N_s and K_s are the numbers of surface species and elementary surface reactions, respectively. For surface species the molar concentration X_j is defined as

$$[X_j] = \Gamma \Theta_j \tag{21}$$

where Θ_i is the surface coverage fraction of species i.

k_{fk}, the forward reaction rate is calculated as

$$k_{fk} = A_k T^{\beta_k} \exp\left(-\frac{E}{RT_s} \right) \prod_{i=1}^{N_s} \Theta_i^{\mu_{ik}} \exp\left(\frac{\varepsilon_{ik} \Theta_i}{RT_s} \right) \tag{22}$$

ε_{ik} and μ_{ik} are the coverage dependence parameters.

For an adsorption process the rate coefficient k_{fk} is computed from S_0 which is the sticking coefficient at vanishing coverage

$$k_{fk} = \left(\frac{S_{0,k}}{(1 - S_{0,k})/2} \right) \frac{1}{(\Gamma)^\tau} \sqrt{\frac{RT}{2\pi M_k}} \tag{23}$$

where τ is the number of sites that the gas phase species k occupies in the adsorption process. In order to trace the temporal evolution of all surface species, a set of ODEs is solved at each flow time step

$$\frac{d\Theta_i}{dt} = \Gamma \dot{R}_{s,i} \quad (i = 1, \ldots, N_s) \tag{24}$$

2.2. The surface and gas phase reactions

The multi-step surface and gas phase reactions mechanisms employed for the oxidation of lean methane–air mixtures on a Pt catalyst are shown in Tables 1 and 2, respectively. The elementary surface reactions have been chosen on the basis of mechanisms proposed by Deutschmann et al. [17], Chou et al. [18] and Aghalayam et al. [19]. However, the values of the pre-exponential (A) or sticking coefficients (S_0) and activation energies (E) for some steps (Table 1)

Table 1
Surface reaction mechanism of oxidation of methane on Pt.

	Reactions	S_0 or A (s^{-1})	β	E (kJ/mol)	μ	ε (kJ/mol)		Ref.
Adsorption reactions								
1	$H_2 + Pt(s) + Pt(s) \rightarrow H(s) + H(s)$	0.046		0.0	−1.0		Pt(s)	[20]
2	$O_2 + Pt(s) + Pt(s) \rightarrow O(s) + O(s)$	0.07 (300/T)		0.0				[20]
3	$CH_4 + Pt(s) + Pt(s) \rightarrow CH_3(s) + H(s)$	0.15		27.0				[18]
4	$CH_4 + O(s) + Pt(s) \rightarrow CH_3(s) + OH(s)$	1.36E+10	0.7	42.0		−8.0	O(s)	[21]
5	$H_2O + Pt(s) \rightarrow H_2O(s)$	0.75		0.0				[20]
6	$CO_2 + Pt(s) \rightarrow CO_2(s)$	0.005		0.0				[20]
7	$CO + Pt(s) \rightarrow CO(s)$	0.84		0.0				[21]
8	$H + Pt(s) \rightarrow H(s)$	1.0		0.0				[17]
9	$O + Pt(s) \rightarrow O(s)$	1.0		0.0				[17]
10	$OH + Pt(s) \rightarrow OH(s)$	1.0		0.0				[17]
Desorption reactions								
11	$H(s) + H(s) \rightarrow Pt(s) + Pt(s) + H_2$	1.0E13		64.4		10.0	H(s)	[20]
12	$O(s) + O(s) \rightarrow Pt(s) + Pt(s) + O_2$	1.0E13		235.0		188.0	O(s)	[20]
13	$H_2O(s) \rightarrow H_2O + Pt(s)$	4.5E12		41.8				[20]
14	$CO_2(s) \rightarrow CO_2 + Pt(s)$	1.0E13		27.1				[20]
15	$CO(s) \rightarrow CO + Pt(s)$	1.0E15		146.0		33.0	CO(s)	[20]
16	$H(s) \rightarrow H + Pt(s)$	6.0E13		254.4		2.8	H(s)	[17]
17	$O(s) \rightarrow O + Pt(s)$	1.0E13		358.8		94.0	O(s)	[17]
18	$OH(s) \rightarrow OH + Pt(s)$	5.0E13		251.1		167.0	O(s)	[17]
Surface reactions								
19	$H(s) + O(s) \rightarrow OH(s) + Pt(s)$	3.5E12		11.2				[20]
20	$OH(s) + Pt(s) \rightarrow H(s) + O(s)$	2.0E12		77.3		73.2	O(s)	[20]
21	$H(s) + OH(s) \rightarrow H_2O(s) + Pt(s)$	5.5E12		66.2				[20]
22	$H_2O(s) + Pt(s) \rightarrow H(s) + OH(s)$	3.1E10		101.4		−167.0	O(s)	[20]
23	$OH(s) + OH(s) \rightarrow H_2O(s) + O(s)$	2.0E12		74.0				[20]
24	$H_2O(s) + O(s) \rightarrow OH(s) + OH(s)$	2.7E11		43.1		−240	O(s)	[20]
25	$C(s) + O(s) \rightarrow CO(s) + Pt(s)$	1.0E11		0.0				[20]
26	$CO(s) + Pt(s) \rightarrow C(s) + O(s)$	1.0E11		236.5		33.0	CO(s)	[20]
27	$CO(s) + O(s) \rightarrow CO_2(s) + Pt(s)$	1.0E11		117.6		33.0	CO(s)	[20]
28	$CO_2(s) + Pt(s) \rightarrow CO(s) + O(s)$	1.0E11		173.3		−94.0	O(s)	[20]
29	$CO(s) + OH(s) \rightarrow CO_2(s) + H(s)$	2.72E10		38.7		33.0	O(s)	[20]
30	$CO_2(s) + H(s) \rightarrow CO(s) + OH(s)$	2.72E10		8.4				[20]
31	$CH_3(s) + Pt(s) \rightarrow CH_2(s) + H(s)$	3.4E13		70.3				[20]
32	$CH_2(s) + H(s) \rightarrow CH_3(s) + Pt(s)$	8.4E13		0.0		2.8	H(s)	[21]
33	$CH_2(s) + Pt(s) \rightarrow CH(s) + H(s)$	2.0E14		58.9		−50.0	C(s)	[20]
34	$CH(s) + H(s) \rightarrow CH_2(s) + Pt(s)$	8.4E13		0.0		2.8	H(s)	[21]
35	$CH(s) + Pt(s) \rightarrow C(s) + H(s)$	8.4E13		0.0		2.8	H(s)	[21]
36	$C(s) + H(s) \rightarrow CH(s) + Pt(s)$	3.4E13		138.0				[20]

Table 2
Gas phase reaction mechanism of oxidation of methane.

	Reactions	A (mol, cm, s^{-1})	β	E (kJ/mol)
1	$O_2 + H = OH + O$	8.70E+13	0	60.3
2	$HO_2 + OH = H_2O + O_2$	6.00E+13	0	0
3	$H + O_2 + M = HO_2 + M$	2.30E+18	−0.8	0
4	$CH_3 + O_2 = CH_2O + OH$	3.30E+11	0	37.4
5	$CHO + M = CO + H$	3.94E+14	0	70.3
6	$CH_4 + OH = H_2O + CH_3$	1.60E+07	1.8	11.6
7	$CO + OH = CO_2 + H$	4.76E+07	1.2	0.29
8	$CH_3 + HO_2 = CH_3O + OH$	1.80E+13	0	0
9	$CHO + O_2 = CO + HO_2$	3.00E+12	0	0
10	$CH_3 + HO_2 = CH_4 + O_2$	3.60E+12	0	0
11	$CH_3O + O_2 = CH_2O + HO_2$	4.00E+10	0	8.9
12	$OH + OH = H_2O + O$	1.50E+09	1.1	0.42
13	$HO_2 + HO_2 = H_2O_2 + O_2$	2.50E+11	0	−5.2
14	$OH + OH + M = H_2O_2 + M$	3.25E+22	−2	0
15	$CO + HO_2 = CO_2 + OH$	1.50E+14	0	98.7
16	$CH_2O + H = CHO + H_2$	2.30E+10	1.1	13.7
17	$CH_2O + OH = CHO + H_2O$	3.40E+09	1.2	−1.9
18	$CH_2O + HO_2 = CHO + H_2O_2$	3.00E+12	0	54.7
19	$CH_2O + O_2 = CHO + HO_2$	6.00E+13	0	170.7
20	$CH_3 + CH_3 = C_2H_6$	8.32E+43	−9.1	67
21	$CH_4 + O = OH + CH_3$	6.92E+08	1.6	35.5
22	$CH_4 + HO_2 = H_2O_2 + CH_3$	1.10E+13	0	103.1
23	$CH_3O + CH_3O \rightarrow CH_3OH + CH_2O$	3.00E+13	0	0
24	$CH_2O + CH_3O \rightarrow CH_3OH + CHO$	6.00E+11	0	13.8
25	$CH_3O_2 + M \rightarrow CH_3 + O_2$	7.24E+16	0	111.1
26	$CH_3 + O_2 + M \rightarrow CH_3O_2 + M$	1.41E+16	0	−4.6
27	$CH_3O_2 + HO_2 \rightarrow CH_3O_2H + O_2$	4.60E+10	0	−10.9
28	$CH_3OH + OH = CH_2OH + H_2O$	1.00E+13	0	7.1

have been selected from Refs. [18,20,21] as they are more relevant for the temperature and concentration ranges considered in the present application. The values of enthalpies of adsorbed species were obtained from Ref. [22]. The reaction mechanism for oxidation of methane in the gas phase (Table 2) [23] has been shown to be adequate for oxidation of lean mixtures of methane with the equivalence ratio of 0.05–0.75 and a temperature range of 900–1400 K [23,24].

3. Numerical solution

The governing equations (Eqs. (1)–(6)) for a packed-bed reactor could not be solved directly using the commercial software Fluent. However, some features of this code such as QUICK scheme and second order method for discretization of temporal terms and easier post-processing of the numerical results are attractive to choose the code for solving Eqs. (1)–(6).

The heat and mass transfer coefficients (e.g. Eqs (10) and (11)) which are not predefined in the software, were computed via modifying subroutines (UDFs). The values for these coefficients were updated at every flow time step. In order to solve the system of ODEs of the equation (24), CVODE integrator [26] was implemented in these subroutines. At each flow time step, Δt, the numerical integration of this system was performed while the flow variables were considered to remain unchanged. Therefore, the rate of depletion or generation of the gas phase species i due to the surface reactions

in this time interval is

$$\dot{R}_{s,i} = \frac{X_{g,i_g}^{t+\Delta t} - X_{g,i_g}^{t}}{\Delta t} \quad (25)$$

This value was then substituted in Eqs. (3) and (4) for numerical solution. Correspondingly, the amount of heat release due to surface reactions (Eq. (5)) was calculated. The same procedure of integration was performed for the gas phase reactions (Eq. (19)). The steady state solution for each condition was sought using the system of equations that nevertheless are in transient form. This was done by performing an adequate number of iterations until the solution reached a steady state operating point. 800 computational cells for spatial discretization of the domain and a time step of 10^{-5} s were used in the simulations.

The parameter a_c in Eqs. (2) and (5) includes the effect of the catalyst loading. This parameter represents the ratio of the catalytic surface area to volume of the reactor. The value of a_c was derived on the basis of comparison with the corresponding experimental data. It was concluded that the catalytic active surface area is 2.31 times the geometric surface area. This value was then used in the rest of the modeling.

To validate the developed model, experimental data we obtained earlier for the oxidation of lean methane–air mixtures in a packed-bed adiabatic reactor with Pt catalyst were used [14]. The simulations were then conducted for the same operational conditions in the same reactor as those employed in the experimental investigation. The reactor bed inside diameter is 0.028 m and the length is 5 cm, with a bed porosity of 0.4. The catalyst used is polycrystalline Pt deposited on Al_2O_3 substrate in the form of cylindrical pellets with both length and diameter of 3.2 mm. The pellet (Al_2O_3) density, specific heat and surface emissivity were, respectively 100 kg/m^3, 837 J/(kg K) and 0.6. The thermal conductivity of Al_2O_3 is considered to be temperature dependent and when the thermal contact resistance between the pellets is taken into account [25], the thermal conductivity of the solid phase varies between 0.48 and 0.41 W/mK when the temperature changes from 700 to 1600 K. The site density, Γ, was assumed to be 2.72×10^{-9} mol/cm^2 which is used for polycrystalline Pt [17]. Pressure along the reactor was assumed to be 89 kPa, the same as in the experiments (local atmospheric pressure in Calgary). Moreover, to validate the gas phase reaction mechanism employed in the model, the simulations were also conducted for comparative purposes for an inert bed reactor.

4. Results and discussion

4.1. Model validation

Fig. 2 shows a comparison of the calculated methane conversion rates with those measured experimentally [14] for a lean mixture with an equivalence ratio, $\Phi = 0.35$ and an approach velocity of 1.0 m/s (space velocity = 7.2×10^4 m^3/(m^3 h) at a reference temperature of 293 K) both for catalytic and non-catalytic adiabatic beds. It can be seen that for the inert bed the experimental value of the ignition temperature of methane is approximately 1070 K which is relatively close to the predicted value of 1125 K. The calculated values of methane conversion in the catalytic bed for different initial temperatures are also in a very good agreement with those obtained experimentally. Moreover, the simulations showed (Fig. 2) that within this bed gas phase reactions have negligible effect on methane conversion at inlet temperatures below 850 K (the solid line in Fig. 2 represents the results obtained using multi-step reaction mechanisms for both the surface and gas phase reactions, while the broken line represents the results when only surface reactions were considered). However, the gas phase reactions become important at higher inlet temperatures.

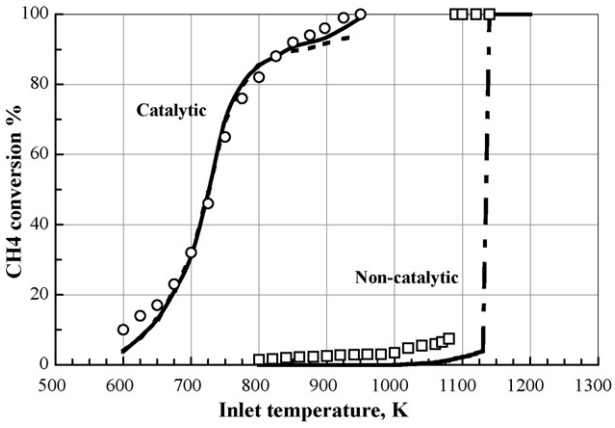

Fig. 2. Methane conversion as a function of inlet temperature within catalytic and non-catalytic beds at $\Phi = 0.35$ and $V_{in} = 1.0$ m/s (space velocity = 7.2×10^4 m^3/(m^3 h)).

The developed model was used to investigate the effects of some key operational conditions such as inlet temperature, approach velocity and equivalence ratio on the methane conversion within lean methane–air mixtures. Moreover, the composition and temperature of the gas mixture along the bed were calculated as well as the heat release rates.

4.2. The effect of inlet temperature

The effect of the inlet temperature on methane oxidation within the adiabatic catalytic reactor is shown in Figs. 3 and 4 for different mixture equivalence ratios and various approach velocities. For comparison, the results of simulations obtained for the inert bed (bare γ-alumina pellets) at the same operational conditions are also presented. It can be seen that the effect of the inlet temperature on the extent of methane oxidation within the catalytic bed depends on the mixture equivalence ratio as shown in Fig. 4. The methane conversion vs. temperature curves are much steeper at higher equivalence ratio. In the inert bed the mixture ignition and complete methane combustion takes place at almost the same temperatures which are in agreement with the experimental observations [14].

4.3. Effect of inlet velocity

It can be seen (Fig. 5) that the value of the mixture inlet velocity has a very significant effect on the oxidation of methane in both types of beds. As expected, the increase in the value of the inlet velocity leads to an increase of the inlet temperature required for complete methane oxidation in both types of beds (Fig. 3). Moreover, it can be seen that the effect of the inlet velocity changing from 0.5 to 15.0 m/s on the extent of methane oxidation within the catalytic bed depends also on the level of the inlet temperature as shown in Fig. 5 for a mixture of equivalence ratio $\Phi = 0.35$. It is to be noted that the effect of the velocity is more pronounced for inlet temperatures within the range of 650–800 K. This temperature range corresponds to the so-called transition region from the regime of kinetically controlled surface reactions (with fuel conversion of up to 20%) to the regime controlled by the mass transport of reactants to the catalytic surface (with fuel conversion of 30–70%). At the low inlet velocity of 0.5 m/s the extent of methane conversion is quite significant even at relatively low inlet temperatures (~88% at 700 K and ~65% at 650 K). However, with an increase in the inlet velocity to 1.0 m/s the methane conversion drops dramatically at

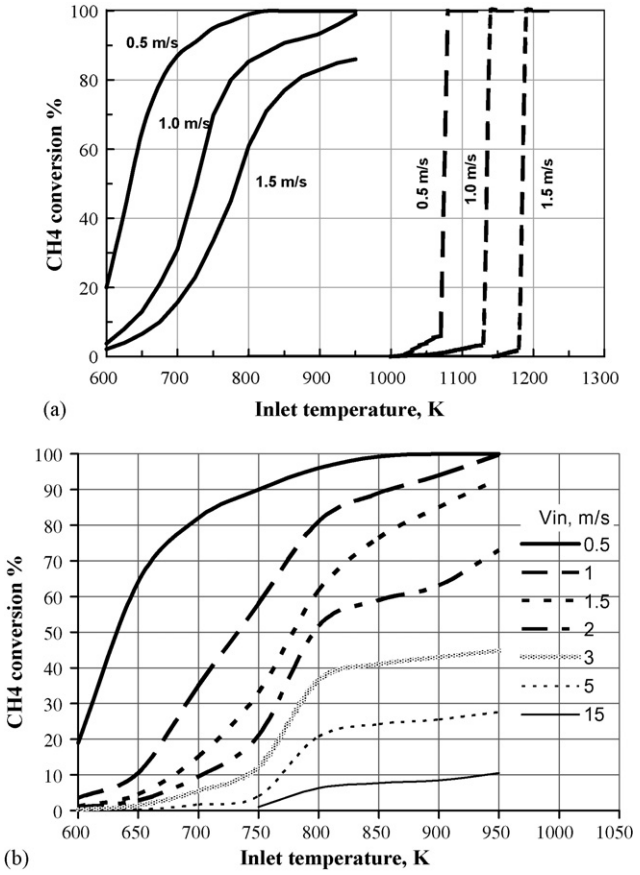

Fig. 3. (a) Methane conversion as a function of inlet temperature within catalytic and non-catalytic beds at different inlet velocities (0.5, 1.0 and 1.5 m/s) and Φ = 0.35; —, catalytic; – – –, non-catalytic. (b) Methane conversion as a function of inlet temperature within catalytic bed over the range of inlet velocities from 0.5 to 15.0 m/s; Φ = 0.35.

the same temperatures to ~32% and 16%, respectively. It appears that a further increase in the inlet velocity to 15 m/s has an insignificant effect on the conversion at these inlet temperatures. The values of inlet temperatures important in catalytic oxidation are summarized in Table 3 for Φ = 0.35 and the inlet velocities V_{in} = 0.5, 1.0 and 1.5 m/s.

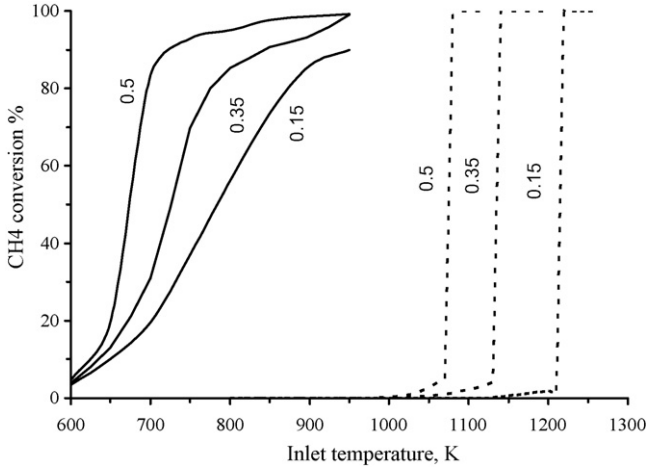

Fig. 4. Methane conversion as a function of inlet temperature within catalytic and non-catalytic beds at different equivalence ratios and V_{in} = 1.0 m/s (space velocity = 7.2 × 10⁴ m³/(m³ h)).

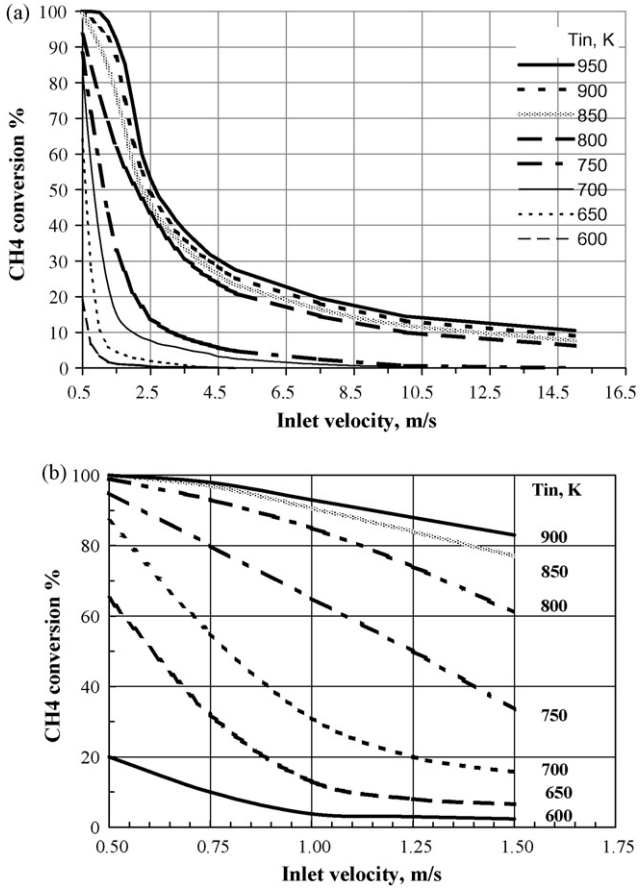

Fig. 5. (a) Methane conversion as a function of inlet velocity at different inlet temperatures and Φ = 0.35. (b) Methane conversion as a function of inlet velocity (up to 1.5 m/s) at different inlet temperatures and Φ = 0.35.

Table 3
Inlet temperatures (K) for 30%, 50%, 90% and 100% methane conversion, Φ = 0.35.

V_{in} (m/s)	Catalytic				Non-catalytic
	$T_{30\%}$	$T_{50\%}$	$T_{90\%}$	$T_{100\%}$	$T_{100\%}$
0.5	611	633	718	812	1075
1	697	726	843	950	1150
1.5	741	782	961	1080	1200

4.4. Effect of equivalence ratio

The effect of mixture equivalence ratio on the extent of methane conversion in the catalytic and non-catalytic beds is shown in Fig. 4 for the inlet velocity of 1.0 m/s. In both cases within the range of equivalence ratios considered (Φ = 0.15–0.50), leaner mixtures needed higher inlet temperatures for ignition and complete combustion (see also Table 4). In the case of the catalytic bed, the effect of the mixture equivalence ratio depends on the level of the inlet temperature, as can be seen in Fig. 6 where the most

Table 4
Inlet temperatures for 30%, 50%, 90% and 100% methane conversion within catalytic and non-catalytic beds; V_{in} = 1 m/s.

Equivalence ratio	Catalytic				Non-catalytic
	$T_{30\%}$	$T_{50\%}$	$T_{90\%}$	$T_{100\%}$	$T_{100\%}$
0.15	730	783	931	1005	1225
0.35	697	726	843	950	1150
0.5	654	663	725	912	1075

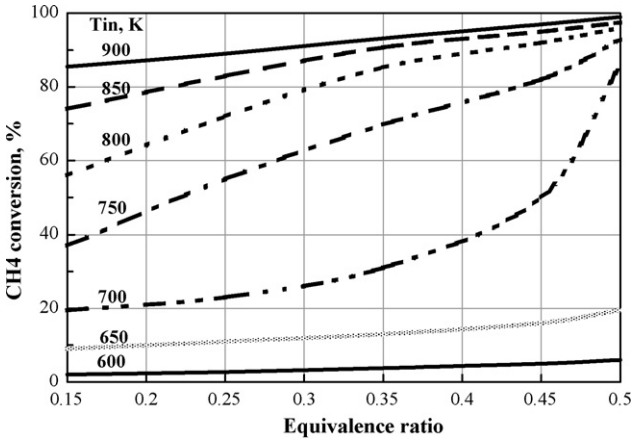

Fig. 6. Methane conversion as a function of equivalence ratio at different inlet temperatures and V_{in} = 1.0 m/s (space velocity = 7.2 × 10^4 m^3/(m^3 h)).

pronounced effect is observed within the range of 700–800 K. At the relatively low inlet temperature of 700 K, an increase in mixture equivalence ratio from 0.15 to 0.35 results in a small increase in methane conversion from ~20% to ~28%. However, a further increase in equivalence ratio from 0.35 to 0.50 produces a significant increase in the methane conversion (from ~45% at Φ = 0.45 to ~75% at Φ = 0.50). The values of inlet temperatures corresponding to 30%, 50%, 90% and 100% methane conversion are summarized in Table 4 for the inlet velocity V_{in} = 1.0 m/s and equivalence ratios Φ = 0.15, 0.35 and 0.50.

4.5. Temperature and species distribution along the bed

The model developed allows calculation of the depletion of methane and formation of products along the catalytic bed. This can be useful information in an analysis of the processes of catalytic oxidation within the bed. The development of CH_4, CO_2 and CO concentrations and temperature profiles along the bed for mixture inlet temperatures of 750 and 900 K are shown in Figs. 7 and 8 correspondingly for equivalence ratio of 0.35 for three different inlet velocities. The hydrogen concentration is not included in the figures since its calculated values are negligible (less than 10^{-6}%). At the relatively low inlet temperature of 750 K (Fig. 7), the methane conversion within the reactor varies significantly with the inlet velocity which controls the residence time. It is 88.2% at the inlet velocity of 0.5 m/s and 33% at the velocity of 1.5 m/s. A small CO concentration of 0.3% was observed at the exit at the low inlet velocity of 0.5 m/s.

Table 5
Temperature and concentrations of CH_4 and CO at exhaust from catalytic bed, Φ = 0.35.

T_{in} (K)	Exhaust	Inlet velocity (m/s)		
		0.5	1	1.5
750	CH_4%	0.41	1.52	2.36
	CO%	0.32	0.14	0.02
	T_{ex} (K)	1451	1210	1021
900	CH_4%	0.026	0.31	0.73
	CO%	0.18	0.49	0.42
	T_{ex} (K)	1507	1470	1398

At the higher inlet temperature of 900 K, the CO concentrations in the exhaust are higher than those for T_{in} = 750 K. It is probably a result of the contribution of gas phase reactions that become significant at higher temperatures. The calculated results also show that at the low inlet velocity of 0.5 m/s the CO concentration reaches its maximum value (within ~1/3 of the bed length) and then decreases towards the exit from the reactor. The location of CO maximum concentration corresponds to the location of the end of rapid gas temperature rise. Such a behavior was also observed experimentally [14].

As expected the exhaust temperature depends on the extent of methane oxidation. The higher the conversion of methane the higher is the gas exhaust temperature. The values of the exhaust gas temperature and exhaust concentrations of methane and carbon dioxide are given in Table 5.

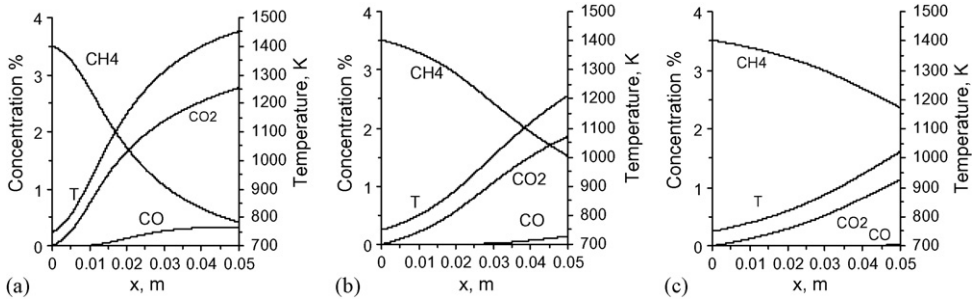

Fig. 7. Species concentrations and gas temperature profiles along catalytic bed at different inlet velocities and T_{in} = 750 K; Φ = 0.35.

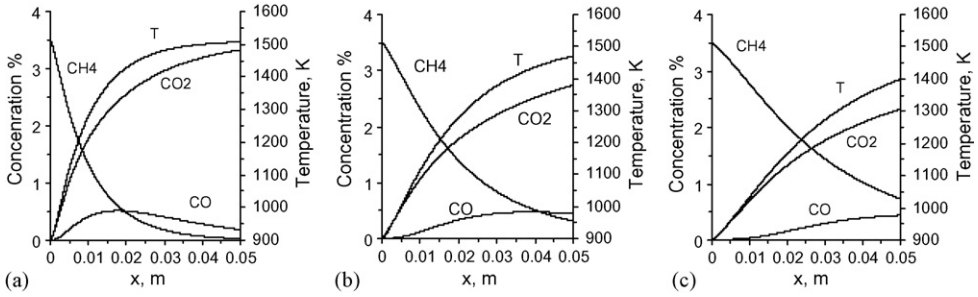

Fig. 8. Species concentrations and gas temperature profile along catalytic bed at different inlet velocities and T_{in} = 900 K; Φ = 0.35.

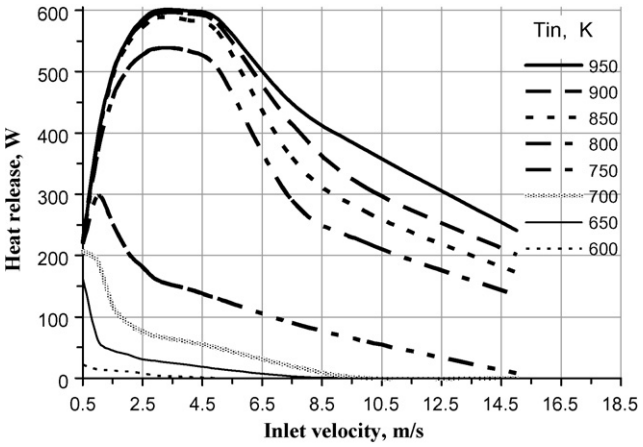

Fig. 9. Heat released (W) as a function of inlet velocity for different inlet temperatures; $\Phi = 0.35$.

4.6. The amount of heat released in the reactor

The heat release in the reactor is the outcome of the effects of changes in the flow rate and the fuel conversion. Increasing the flow rate reduces the residence time that hinders the fuel conversion but can increase the amount of heat release as more fuel flows in the system. Values of heat released for the inlet velocities and temperatures considered in this study are shown in Fig. 9. The maximum amount of heat release, 595 W, takes place at the inlet velocity of 3.0 m/s and the inlet temperature of 900 K. The methane conversion at these conditions is less than 45%. Examining Fig. 5 along with Fig. 9 shows that typically for 80% methane conversion the maximum amount of heat release occurs at the inlet velocity of 2.0 m/s for the inlet temperature of 900 K. Under these inlet conditions the amount of heat release is 545 W. This is comparable to 595 W.

5. Conclusions

The model for simulation of a catalytic oxidation of lean homogeneous methane–air mixtures in a adiabatic packed-bed reactor has been developed employing multi-step surface and gas phase reaction mechanisms. It was demonstrated that the model could predict the effect of changes in operational conditions such as inlet mixture temperature, velocity and equivalence ratio on the methane conversion as well as species concentrations and gas temperature profiles along the bed. The results of calculations were in good agreement with corresponding experimental data.

Acknowledgement

The financial support of NSERC of Canada is greatly appreciated.

References

[1] M.F.M. Zwinkels, S.G. Jaras, P.G. Menon, T.A. Griffin, Catalytic materials for high-temperature combustion, Catalysis Review: Science and Engineering 35 (3) (1993) 319–358.
[2] P. Forzatti, Environmental catalysis for stationary applications, Catalysis Today 62 (2000) 51–65.
[3] R. Prasad, L.A. Kennedy, E. Ruckenstein, Catalytic combustion of propane using transitional metal oxides, Combustion Science and Technology 22 (5 and 6) (1980) 271–280.
[4] L. Urfels, P. Gélin, M. Primet, E. Tena, Complete oxidation of methane at low temperature over Pt catalysts supported on high surface area SnO_2, Topics in Catalysis 30–31 (2001) 427–432.
[5] R.M. Heck, R.J. Farrauto, Automobile exhaust catalysts, Applied Catalysis A: General 221 (2001) 443–457.
[6] G. Groppi, E. Tronconi, P. Forzatti, Mathematical models of catalytic applications, Catalysis Review: Science and Engineering 41 (2) (1999) 22–254.
[7] P. Forzatti, Status and perspectives of catalytic combustion for gas turbines, Catalysis Today 83 (1–4) (2003) 3–18.
[8] S. Tischer, C. Correa, O. Deutschmann, Transient three-dimensional simulations of a catalytic combustion monolith using detailed models for heterogeneous and homogeneous reactions and transport phenomena, Catalysis Today 69 (2001) 57–62.
[9] L.L. Rajaa, R.J. Keea, O. Deutschmannb, J. Warnatz, L.D. Schmidt, A critical evaluation of Navier–Stokes, boundary-layer, and plug-flow models of the flow and chemistry in a catalytic-combustion monolith, Catalysis Today 59 (2000) 47–60.
[10] R. Jahn, D. Snita, M. Kubicek, M. Marek, 3D modeling of monolith reactor, Catalysis Today 38 (1997) 39–46.
[11] S. Salomons, R.E. Hayes, M. Poirier, H. Sapoundjiev, Modeling a reverse flow reactor for the catalytic combustion of fugitive methane emissions, Computers and Chemical Engineering 28 (2004) 1599–1610.
[12] M. Bizzi, L. Basini, G. Saracco, V. Specchia, Short contact time catalytic partial oxidation of methane: analysis of transport phenomena effects, Industrial Engineering Chemical Research 42 (2003) 62–71.
[13] K.L. Hohn, L.D. Schmidt, Partial oxidation of methane to syngas at high space velocities over Rh-coated spheres, Applied Catalysis A: General 211 (2001) 53–69.
[14] I. Wierzba, A. Depiak, The catalytic oxidation of heated lean homogeneously premixed gaseous-fuel air streams, Chemical Engineering Journal 91 (2–3) (2003) 287–294.
[15] B.P. Singh, M. Kaviany, International Journal of Heat and Mass Transfer 35 (6) (1992) 1395–1397.
[16] F. Yoshida, D. Ramswami, O.A. Hougen, Temperatures and partial pressures at the surfaces of catalyst particles, AIChE Journal 8 (1962) 5–11.
[17] O. Deutschmann, L.I. Maier, U. Riedel, A.H. Stroemman, R.W. Dibble, Hydrogen assisted catalytic combustion of methane on platinum, Catalysis Today 59 (2000) 141–150.
[18] C.P. Chou, J.Y. Chen, G.H. Evans, W.S. Winters, Numerical studies of methane catalytic combustion inside a monolith honeycomb reactor using multi-step surface reactions, Combustion Science and Technology 150 (1) (2000) 27.
[19] P. Aghalayam, Y.K. Park, N. Fernandes, V. Papavassiliou, A.B. Mhadeshwar, D.G. Vlachos, A C1 mechanism for methane oxidation on platinum, Journal of Catalysis 213 (1) (2003) 23–38.
[20] D.K. D Zerkle, M.D. Allendorf, M. Wolf, O. Deutschmann, Understanding homogeneous and heterogeneous contributions to the platinum-catalyzed partial oxidation of ethane in a short-contact-time reactor, Journal of Catalysis 196 (1) (2000) 18–39.
[21] R.R. Quiceno, J. Perez Ramirez, J. Warnatz, O. Deutschmann, Modeling the high-temperature catalytic partial oxidation of methane over platinum gauze: detailed gas phase and surface chemistries coupled with 3D flow field simulation, Applied Catalysis A: General 303 (2000) 166–176.
[22] J. Warnatz, M.D. Allendorf, R.J. Kee, M.E. Coltrin, A model for chemistry and fluid mechanics in the combustion of hydrogen on platinum surface, Combustion and Flame 96 (1994) 393–406.
[23] M. Reinke, J. Mantzaras, R. Bombach, S. Schenker, A. Inauen, Gas phase chemistry in catalytic combustion of methane/air mixtures over platinum at pressures of 1 to 16 bar, Combustion and Flame 141 (4) (2005) 448–468.
[24] J. Warnatz, R.W. Dibble, U. Mass, Combustion Physical and Chemical Fundamentals, Modeling and Simulation, Springer–Verlag, New York, 1996, p. 69.
[25] M. Bahrami, M.M. Yovanovich, J.R. Culham, Effective thermal conductivity of rough spherical packed beds, International Journal of Heat and Mass Transfer 49 (19–20) (2006) 3691–3701.
[26] A.C. Hindmarsh, P.N. Brown, K.E. Grant, S.L. Lee, R. Serban, D.E. Shumaker, C.S. Woodward, SUNDIALS: suite of nonlinear and differential/algebraic equation solvers, ACM Transactions on Mathematical Software 31 (3) (2005) 363–396.